DOI: 10.1002/chem.200601722

Characterization of Titanium Dioxide Nanoparticles Dispersed in Organic Ligand Solutions by Using a Diffusion-Ordered Spectroscopy-Based Strategy

Luk Van Lokeren,[a] Géraldine Maheut,[a] François Ribot,[b] Virginie Escax,[a, b] Ingrid Verbruggen,[a] Clément Sanchez,[b] José C. Martins,[c] Monique Biesemans,*[a] and Rudolph Willem[a]

Abstract: Diffusion-ordered NMR spectroscopy (DOSY NMR) is presented as a tool for the determination of the diffusion coefficients of organic ligands in suspensions of titanium dioxide nanoparticles. The nanoparticles were prepared by a sol-gel process by hydrolysis and condensation reactions of titanium tetra-*n*-butoxide in the presence of pentane-2,4-dione (acacH: acetylacetone), as well as *para*-toluenesulfonic acid (*p*TsA) and *n*-butanol (*n*BuOH). NMR spectroscopic studies were performed in various deuterated solvents, on both dispersed xerosols and diluted sols. The bipolar-pulsed field gradient longitudinal eddy-current delay (LED) pulse sequence was used for data acquisition. The data were processed by inverse Laplace transformation (ILT), by using a maximum entropy algorithm, to afford 2D DOSY spectra. Different diffusion regimes for organic ligands in the bound and unbound states were successfully discriminated, more particularly in [D_3]acetonitrile, thus allowing assessment of their interactions with the nanoparticles.

Keywords: diffusion · ligand effects · nanostructures · NMR spectroscopy · titanium dioxide

Introduction

Measuring in situ the affinity between an organic ligand and an inorganic metal-oxide nanoparticle remains a difficult task. Generally, this affinity is measured from adsorption isotherms, quantifying either the organic ligands remaining in the solution freed from the nanoparticles or the organic ligands remaining on the isolated solid. Both approaches require tedious separation protocols (centrifugation, ultrafiltration, etc.), which can be invalidated if the exchange rate of the ligands is faster than the timescale of the separation process. This hampers the ability to gain insight into the actual nature of the interaction phenomena occurring at the surface of the particle. Various standard methods, for example, dynamic light scattering (DLS), enable one to determine the size distribution of particles suspended in solution, but cannot address the issue of the structural nature of the ligand–nanoparticle interactions. The development of new tools to characterize dispersed nanoparticles and to understand these interactions remains a major issue. Pulsed field gradient NMR spectroscopy is an in situ methodology which enables both the resolution and quantification of complex mixtures of different species in solution on the sole basis of their differentiated translational mobility.[1,2] The use of two-dimensional (2D) NMR experiments, which combine a chemical shift scale and a diffusion coefficient scale in so-called 2D diffusion-ordered (DOSY) NMR spectra, provides a straightforward assignment of the diffusion correlation peaks associated with the various molecular species present in the mixture. Therefore, this analytical tool is complementary to conventional separation techniques,[3] for instance, size exclusion chromatography (SEC), in which the

[a] L. Van Lokeren, Dr. G. Maheut, Dr. V. Escax, I. Verbruggen, Prof. Dr. M. Biesemans, Prof. Dr. R. Willem
High Resolution NMR Centre (HNMR)
Vrije Universiteit Brussel
Pleinlaan 2, 1050 Brussel (Belgium)
Fax: (+32) 2-629-3291
E-mail: mbiesema@vub.ac.be

[b] Dr. F. Ribot, Dr. V. Escax, Dr. C. Sanchez
Laboratoire de Chimie de la Matière Condensée de Paris
Université Pierre et Marie Curie - Paris6, CNRS UMR 7574
Tour 54, 5e étage, 4 Place Jussieu
75252 Paris Cedex 05 (France)

[c] Prof. Dr. J. C. Martins
NMR and Structural Analysis Unit
Vakgroep Organische Chemie, Universiteit Gent
Krijgslaan 281 S4, 9000 Gent (Belgium)

Supporting information for this article is available on the WWW under http://www.chemeurj.org/ or from the author.

components of the mixture are separated chemically rather than spectroscopically. It is likewise of major interest for mixtures of soluble or dispersible compounds (surfactants),[4] and products with reduced translational mobility (dendrimers,[5] polymers,[6] and macromolecules[7]) whenever species of different sizes or molar masses are to be distinguished.[8] Another advantage of this methodology is its potential to investigate interactions between various species in solution and to gain insight into their mutual clustering (for example, organic tin-oxide based clusters) as well as their affinity to the solvent.[9,10] More recently, DOSY NMR was explored as a tool for investigating to what extent measuring diffusion coefficients enables ligands grafted to the surface of particles to be distinguished from unbound ones in solution (CeO_2, InP).[11,12] In the case of InP, kinetic aspects of the ligand exchanges involved in association/dissociation equilibria were likewise investigated.[12]

Sanchez and co-workers described the synthesis of soluble,[13] size-tailored nanoparticles of titanium dioxide (anatase)[14] by hydrolysis–condensation reactions of titanium tetra-*n*-butoxide in the presence of pentane-2,4-dionate (acac: acetylacetonate) and *p*-toluenesulfonic acid (*p*TsA) in wet *n*-butanol (*n*BuOH). It is well known that, in solution, acetylacetone (acacH) exists as two distinct species, a ketone and an enol in mutual tautomeric equilibrium. In the case of TiO_2, only the deprotonated enolic tautomer can act as a bidentate complexing agent for the nanoparticle. This system appeared to be a particularly relevant and experimentally suitable model for translational mobility investigations on nanoparticles by DOSY NMR, given that TiO_2 enjoys a wide range of applications and its properties are well described and easily controllable as far as the particle size is concerned. We focused more particularly on the so-called S_3 sol featuring nanoparticles with diameters ranging from approximately 2 to 6 nm, the size of which depends on the sample preparation conditions, as revealed previously by DLS.[13] The xerogel was obtained by drying this sol, and was thoroughly investigated by DOSY NMR. We believed that 2D DOSY ^{1}H NMR spectra would enable us to address ligand-exchange phenomena taking place at the surface of the titanium dioxide nanoparticles and possible interactions between the reagents present in the saturated "sol" medium, as well as in the re-dispersed xerosol.[15] In order not to overlook any possible interaction between reagents and/or solvent molecules, DOSY NMR experiments were also performed on so-called blanks, prepared under exactly the same conditions as the above-mentioned sols except that titanium tetra-*n*-butoxide was substituted for pure *n*BuOH. Herein, we present the successful achievement of these goals.

Results and Discussion

Methodological considerations: In solution, only translational motions enable one to determine the diffusion coefficient by using the Debye–Einstein equation [Eq. (1)]:

$$D = k_B T / f_T \quad (1)$$

in which k_B is the Boltzmann constant, T the temperature in Kelvin and f_T the friction factor. Assuming the diffusing structural unit has a spherical shape, Equation (1) can be rewritten as the well-known Stokes–Einstein equation [Eq. (2)][16]:

$$D = k_B T / c\pi\eta r_H \quad (2)$$

in which η is the viscosity of the solvent, r_H is the hydrodynamic radius of the structural unit and c is a parameter that goes asymptotically to six as the hydrodynamic radius increases, which is generally achieved for structures with a diameter of 1 nm or more.[17]

Equation (2) is convenient to estimate the molecular radii of species in solution from diffusion coefficient measurements. Given that structural units generally do not have a spherical shape, the hydrodynamic radius r_H deduced from a diffusion coefficient measurement by using Equation (2) should simply be considered as the radius of a fictitious, spherical structural unit, which diffuses with the same translational rate as the structural unit under investigation.

In a first stage, the DOSY measurements were performed on model solutions prepared from tetramethylsilane (TMS) and only a single component involved in the sol or xerosol, namely, acacH, *n*BuOH, or *p*TsA in a given deuterated solvent. Subsequently, DOSY experiments were conducted for the three types of samples of interest—blank, sol S_3, and xerosol X_3—in the same solvent. Comparison of the diffusion coefficients of the species in these model solutions with those in the blank solutions, in which all the components are present apart from the nanoparticles under identical conditions of concentration, provides valuable information as to their possible mutual interactions, independent of their possible interactions with the nanoparticles.

It is convenient to circumvent changes of viscosity from one sample to another by defining a reduced diffusion coefficient $\Delta_{j(S)}$ as the ratio of the diffusion coefficient of the species j in sample S of interest to that of TMS in the same sample [Eq. (3)]. TMS is a nonpolar and nonpolarizable species, and is therefore presumed to have diffusive properties, which are sensitive only to the viscosity of the sample and not to any other interaction (j: acacH, *n*BuOH, *p*TsA; S: models, blank, S_3, X_3):[18]

$$\Delta_{j(S)} = D_{j(S)} / D_{TMS(S)} \quad (3)$$

The quantity $\Delta_{j(S)}$ thus provides information on the sensitivity of the diffusion of species j in sample S to the polarity of the medium, as well as on other possible interactions in which the species j might be involved.

The timescale to separate fast from slow exchange is different in DOSY NMR compared with regular 1D NMR spectroscopy. In DOSY the timescale to be considered is the diffusion time used in between the coding and decoding gra-

dient pulses (that is, about 100–200 ms in the experiments reported here), while for 1D NMR spectroscopy the timescale corresponds to the inverse of the frequency difference in between the two chemical shifts of the species concerned (that is, for a $\delta =$ 0.5 ppm difference at 250 MHz, the characteristic time for the coalescence is about 8 ms).

Table 1. Diffusion coefficients[a] [10^{-10} $m^2 s^{-1}$] and reduced diffusion coefficients, in [D_3]acetonitrile, for the pure compounds (model solutions), blank sample, and redispersed xerosol X_3. The relative fractions are also given for species in different states (for example, free and bound).

Compounds		Model solutions		Blank		X_3		
		$D_{j(model)}$	$\Delta_{j(model)}$	$D_{j(blank)}$	$\Delta_{j(blank)}$	$D_{j(X3)}$	$\Delta_{j(X3)}$	%
*p*TsA	free	15.9	0.55	10.2	0.43			
	hindered/free					9.7	0.27	50
	bound					4.3	0.12	50
enolic 60%	free acacH	29.1	0.97	24.1	1.02	29.0	0.81	85
	bound acac					3.4	0.09	15
ketonic 40%	free acacH	27.2	0.91	21.7	0.92	27.5	0.76	100
*n*BuOH	free	28.7	0.94	20.6	0.87	30.4	0.84	100
TMS	free	29.8	1.00	23.6	1.00	36.0	1.00	100

[a] The relative accuracy of the diffusion coefficients is ±1% for models, ±1% for the blank, and ±10% for X_3, and the relative accuracy of the fractions determined from DOSY NMR is ±10% (see the Experimental Section).

Evidence for chemical reactions in the blank: Apart from the expected diffusion correlation peaks from the species of interest (*p*TsA, acacH/acac, and *n*BuOH), the 2D DOSY ^{1}H NMR spectrum of the blank solution shows some additional peaks. In the singlet methyl area of the blank solution in CD_3CN, an additional unexpected diffusion correlation peak is observed with a chemical shift ($\delta = 2.10$ ppm) between those of the enolic ($\delta = 2.01$ ppm) and ketonic ($\delta =$ 2.15 ppm) tautomers of acacH, which arises from a species not observed in any of the spectra of the pure components. This additional compound appears to be acetone generated as a degradation product upon mixing the different components of the blank solutions. This byproduct is obtained most likely by decomposition of acacH by a retro-Claisen reaction. This reaction also produces acetic acid, which reacts further with free *n*BuOH to yield *n*-butyl acetate, of which only the α-CH_2 butyl resonances are well resolved at $\delta = 4.02$ ppm. The resonance of the methyl moiety of the acetyl group and the other *n*-butyl resonances overlap at 250 MHz with the resonances of the residual solvent ($\delta =$ 1.94 ppm) and the *n*BuOH. However, a ^{1}H NMR spectrum acquired at 700 MHz clearly shows the resonances of the acetyl group at $\delta = 1.97$ ppm and of the β-CH_2 at $\delta =$ 1.58 ppm. The γ-CH_2 and the methyl resonances of *n*-butyl acetate are also visible in the spectrum, but only partially as shoulders of the corresponding *n*BuOH resonances. Finally, it also appears that acetone is partially reduced further into isopropanol, as revealed by the two characteristic multiplet resonances at $\delta = 1.09$ and 3.86 ppm.

Some additional unidentified, variably broad resonances, which appear with poorly reproducible chemical shifts in the spectrum, coalesce away upon addition of [D_4]methanol, indicating that these resonances originate from chemically exchangeable protons, mostly hydroxylic ones.

DOSY NMR investigations in [D_3]acetonitrile: The diffusion coefficients of the different species, as obtained from the model solutions of the pure organic compounds, the blank and the redispersed xerosol X_3 in CD_3CN, are collected in Table 1. Here, the data indicate that, apart from *p*TsA, all other species display rather similar reduced diffusion coefficients in the model solutions and in the blank. Therefore, the change of diffusion behavior of each species when switching from model to blank is mostly related to the viscosity change. The enolic acacH tautomer ($D_{blank} = 24.1 \times 10^{-10}$ $m^2 s^{-1}$) diffuses slightly faster than the ketonic one ($D_{blank} = 21.7 \times 10^{-10}$ $m^2 s^{-1}$) in the blank, which appears already to be the case in model solutions. As compared to the others, the *p*TsA species diffuses markedly slower than TMS in the model solution. The size of acacH and *p*TsA being similar,[19] the slower diffusion of *p*TsA is likely to be related to aggregation phenomena through dipole–dipole interactions, π stacking, and/or hydrogen bonds. The presence of acacH and *n*BuOH in the blank slows down further, albeit slightly, the translational diffusion of *p*TsA, which is not surprising in view of the hydrogen bridge donor capacities of acacH and *n*BuOH. That the diffusion coefficients of the latter two substances remain roughly unaffected by the presence of *p*TsA appears acceptable, as both acacH and *n*BuOH are present in large molar excess with respect to *p*TsA (acacH/*p*TsA 15:1, *n*BuOH/*p*TsA 50:1), which, accordingly, has to be much more sensitive to intermolecular interactions from other species.

The 1D ^{1}H NMR spectra of the redispersed xerosol X_3 and of the sol S_3 in [D_3]acetonitrile display novel resonances not observed in the blank (Figure 1). The observed AA′XX′ line pattern for the aromatic protons of *p*TsA, appearing as two doublets with reasonably sharp resonances in the blank, is somewhat broadened in X_3 and S_3. It is accompanied by additional very broad resonances at the low (X_3) and the high (S_3) frequency sides. These additional broad bands, extending well over $\delta = 0.2$ ppm, are assigned to the *p*TsA ligands interacting directly with TiO_2 nanoparticles, as evidenced from their slower translational diffusion measured by 2D DOSY (Figure 2). The resulting slower rotational reorientation rate of the ligands interacting directly (or indirectly) with the nanoparticles explains this dramatic line broadening. The relative displacement of the broad bands with respect to the narrower doublets, from X_3 to S_3, is most likely related to the presence of *n*BuOH in large excess in S_3.

The overlapping and broadened resonances in the aromatic, as well as in the methyl, spectral range of *p*TsA in both

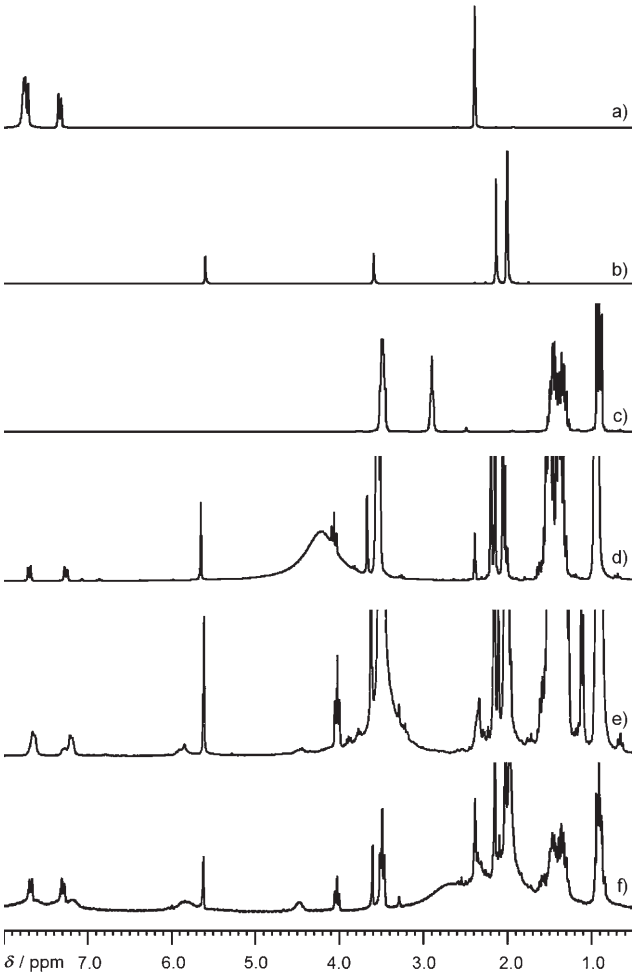

Figure 1. 1D ^{1}H NMR spectra of model solutions; a) *p*TsA, b) acacH, c) *n*BuOH, d) blank, e) S_3, and f) X_3 in [D_3]acetonitrile.

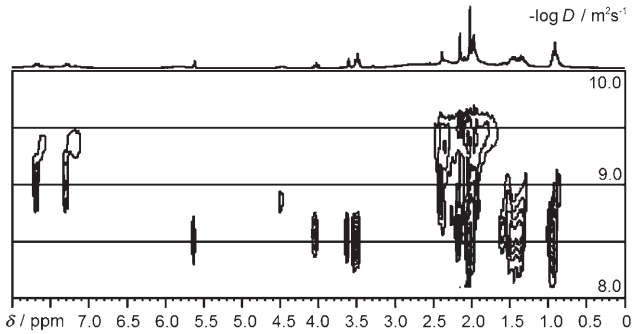

Figure 2. Complete 2D DOSY spectrum of xerosol X_3 redispersed in [D_3]acetonitrile, with projection along the chemical shift axis.

X_3 and S_3 can clearly only originate from the presence of the TiO_2 nanoparticles, as such broadened resonances are completely absent in the blank solution (Figure 1). The diffusion coefficient analysis resulting from the 2D DOSY spectrum of the xerosol X_3 is presented in Table 1, and some of the corresponding spectral ranges of interest are displayed in Figures 3, 4, and 5.

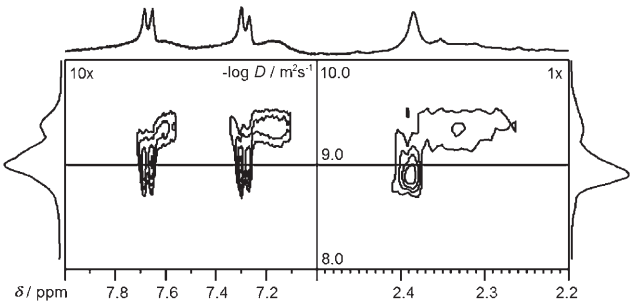

Figure 3. Aromatic and methyl proton resonance ranges of the *p*TsA ligand in the 2D DOSY spectrum of xerosol X_3 redispersed in [D_3]acetonitrile, with projections along the chemical shift and diffusion axes. Contour levels and projections are not identical in the left (10×) and right (1×) panels, for the sake of optimal representation.

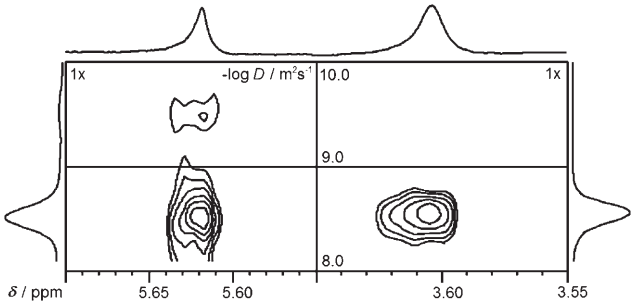

Figure 4. Vinylic spectral range of the enolic tautomer (left panel) and methylene spectral range of the ketonic tautomer (right panel) of acac(H) in the 2D DOSY spectrum of the xerosol X_3 redispersed in [D_3]acetonitrile, with projections along the chemical shift and diffusion axes.

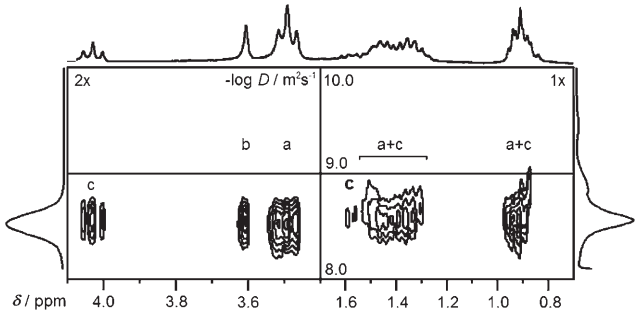

Figure 5. Spectral expansions in the 2D DOSY spectrum of the xerosol X_3 redispersed in [D_3]acetonitrile, with projections along the chemical shift and diffusion axes, in the resonance ranges of *n*BuOH (a), ketonic acacH (b), and *n*-butyl acetate (c), a byproduct generated in situ. The *n*-butyl acetate is clearly visible with low-intensity diffusion correlation multiplets around $\delta = 1.59$ (β-CH_2 (*n*-butyl acetate), right panel) and 4.02 ppm (α-CH_2 (*n*-butyl acetate), left panel); the correlation peaks in the range $\delta = 1.25$–1.55 ppm are assigned to β-CH_2 (*n*BuOH) and γ-CH_2 (*n*BuOH, *n*-butyl acetate) moieties (right panel). The diffusion correlation multiplets around $\delta = 3.49$ (left panel) and 0.9 ppm (right panel) correspond to the α-CH_2 (*n*BuOH) and CH_3 (*n*BuOH, *n*-butyl acetate) moieties, respectively. Contour levels and projections are not identical in the left (2×) and right (1×) panels, for the sake of optimal representation.

Integration of the resonances of the enolic and ketonic tautomers of acacH, in the standard 1D spectrum, enables

one to deduce that approximately 60% of the acacH in the mixture appears in enolic form, and thus only approximately 40% is in the ketonic form.

Figures 3 and 4 (left panel) clearly reveal the presence of 2D DOSY diffusion correlation peaks lying in the reasonably narrow range of $-\log D$ values between 9.3 and 9.6, even though they are considerably smeared out along the horizontal chemical shift axis, as a consequence of the line broadening resulting from slowed down rotational molecular dynamics. In particular, the *p*TsA ligand gives rise to a broad $-\log D$ range centered between 9.3 and 9.5 for both aromatic proton resonances ($\delta = 7.0$–7.6 ppm) as well as for the methyl singlet ($\delta = 2.2$–2.4 ppm; Figure 3). Analogously, the enolic acac ligand gives rise to two rather well-defined diffusion correlation peaks in the $-\log D$ range between 9.4 and 9.6, as found at the cross section of the 2D DOSY spectrum for both the vinylic (at $\delta = 5.62$ ppm; Figure 4, left panel) and methylic (at $\delta = 2.02$ ppm; not shown) resonances of the enolic acac(H) ligand. By contrast, the ketonic acacH (Figure 4, right panel) and *n*BuOH resonances (Figure 5) do not show any DOSY diffusion correlation peak at all in the range $9.3 < -\log D < 9.6$, which clearly demonstrates that none of them plays a specific role in the functionalization of the titanium dioxide nanoparticles. As further shown in Figure 5, the diffusion correlation multiplets around $\delta = 1.59$ (right panel) and 4.03 ppm (left panel) arise only from *n*-butyl acetate, while the correlation multiplets around $\delta =$ 3.49 (right panel) and 0.9 ppm (left panel) only arise from *n*BuOH. All other resonances arise jointly from both *n*-butyl acetate and *n*BuOH, resulting in the observable peak dispersion along the diffusion axis. Although only a minor fraction, *n*-butyl acetate as a byproduct displays two observable diffusion correlation multiplets that are sufficiently separated to reveal a diffusion coefficient slightly lower than that for *n*BuOH.

Slowly diffusing species provide diffusion cross-peaks in the range $9.3 < -\log D < 9.6$, which corresponds to a range of 5×10^{-10} to $2.5 \times 10^{-10}\ m^2 s^{-1}$ for the diffusion coefficients and to a range of 1.5–3.0 nm for the hydrodynamic radii ($\eta =$ 0.29 cP). Such a hydrodynamic radius range is in excellent agreement with the radii of TiO_2 nanoparticles determined previously for the present system by DLS, and confirms their reasonably narrow size distribution.[13]

The assignment of the enolic and ketonic acac(H) resonances is straightforward. Both forms exhibit diffusion correlation peaks for all their resonances in the $-\log D$ range around 8.5, with diffusion coefficients of 2.90×10^{-9} and $2.75 \times 10^{-9}\ m^2 s^{-1}$ for enolic and ketonic acacH, respectively, characteristic of unbound, free-moving ligands. Only the enolic acac tautomer additionally exhibits diffusion correlation peaks around $-\log D = 9.5$ ($3.4 \times 10^{-10}\ m^2 s^{-1}$), characteristic of the bound ligand. This unambiguously confirms that the enolic acac ligand is basically the only form of acac that chelates the Ti atoms at the nanoparticle surface. The two separated diffusion correlation peaks observed for enolic acac, on the other hand, enable one to conclude that its bound and free forms undergo an association–dissociation exchange in which the ligand remains bound to the surface for an average time that is longer than the diffusion time used in the bipolar pulse pair–longitudinal eddy-current delay (BPP-LED) sequence, that is, 100–200 ms. Stated in other terms, the exchange kinetics are slow on the diffusional timescale.

The reduced diffusion coefficient for *n*BuOH in X_3 is very similar to that observed in the blank (Table 1), indicating that interactions with the nanoparticles are negligible. In the case of the ketonic acacH, its reduced diffusion coefficient in X_3 is decreased by approximately 20% as compared to the blank (Table 1). This result suggests that ketonic acacH exists essentially in free form, but might undergo some slowing down in its diffusion due to the presence of the nanoparticles. According to the very small volume fraction occupied by the particles (estimated at approximately 1% maximum for 10 mg of X_3 in 750 μL of solvent), obstruction effects should be negligible.[7] Alternatively, a small fraction of the ketonic acacH might be bound to the nanoparticles under a fast exchange regime (for example, with an interaction time shorter than 100–200 ms) with the corresponding bulk species. The same argument holds for the free enolic ligand, the reduced diffusion coefficient of which is also decreased by approximately 20% when comparing X_3 to the blank (Table 1). Globally, this apparent slowing down of ligands not strongly bound to nanoparticles remains a minor, though significant, effect (see further discussion below).

Deconvolution of the volume of the diffusion correlation peaks of acac/acacH as a function of the diffusion coefficient allows the estimation that roughly 5 to 25% of the enolic form is bound as acac to the surface of the nanoparticles. By contrast, as for the blank, the behavior of the *p*TsA ligand again deserves special focus. The result of a twice as large relative hydrodynamic radius for *p*TsA when compared to *n*BuOH and both tautomers of acacH (Table 1) is even amplified for the xerosol X_3, the reduced diffusion coefficient for the "faster" *p*TsA fraction (labeled "hindered/free" in Table 1) going down to 0.27. This particular *p*TsA fraction is different from the tightly nanoparticle-bound fraction, which exhibits an even smaller reduced diffusion coefficient (0.12) and a well-separated diffusion correlation peak on both diffusion and chemical shift scales in the aromatic region. This "hindered/free" *p*TsA is ascribed to an exchange between the free aggregate complex, as observed in the blank, and an alternative hindered form which is loosely but significantly experiencing the influence of the slower diffusion of the nanoparticles, this exchange now being fast on both the chemical shift and diffusion timescales. The validity of this interpretation is evidenced by the fact that all the resonances in both the aromatic and methylic regions exhibit diffusion correlation peaks in the same $-\log D$ range and also appear in the 1D spectrum as resonances displaying significant broadening with respect to the blank solution (Figure 1). In particular, this broadening reflects a fast exchange between the *p*TsA ligand with a diffusive pattern typical to the blank, and another slowed down species, which, however, cannot be *p*TsA strongly bound to the

nanoparticles. The interactions between the nanoparticles and these hindered species may be of electrostatic and/or dipolar nature, and are sufficiently strong to influence their diffusion rates, but are too weak to prevent fast exchange with the *p*TsA ligands in the bulk solution.

Deconvolution of the correlation peaks summed along the diffusion axis in the chemical shift ranges 7.80–7.00 or 2.45–2.25 ppm reveals that between 40 and 60% of *p*TsA ligands are tightly bound to the surface of the nanoparticles ($9.3 < -\log D < 9.5$), while the remaining fraction ($8.8 < -\log D < 9.1$) is in fast exchange between the pool of loosely bound *p*TsA ligands (hindered) and the free ones.

The slow diffusion regimes of both enolic acac and *p*TsA ($9.3 < -\log D < 9.6$) clearly correspond to a strongly nanoparticle-bound state. Thus, it seems unrealistic that an averaged diffusion coefficient from a hypothetical fast diffusion-exchange regime would result in virtually identical values for ligands as different as *p*TsA and enolic acac, certainly in view of their very different concentrations. Furthermore, both *p*TsA and enolic acac ligands do exhibit other 2D DOSY diffusion correlation peaks in other, faster but different diffusion regimes, as discussed below. Last but not least, as stated above, the resulting estimated hydrodynamic radii appear to match very well the numerical values from DLS.[13]

For the "faster" fraction of *p*TsA ligands not tightly bound to the nanoparticles, an averaged diffusion constant can be defined as [Eq. (4)]:

$$< D >_{X3} = x_{f(X3)} D_{f(X3)} + x_{h(X3)} D_{h(X3)} \quad (4)$$

in which $D_{f(X3)}$ and $x_{f(X3)}$ refer, respectively, to the diffusion coefficient and the molar fraction of the free ligand fraction, while $D_{h(X3)}$ and $x_{h(X3)}$ refer to those of the hindered ligand fraction of *p*TsA. In Equation (4), the quantity $< D >_{X3}$ is the experimentally measured parameter, and when considering only the pool of *p*TsA ligands not tightly bound to the nanoparticles, $x_{f(X3)} + x_{h(X3)} = 1$. $D_{h(X3)}$ is not directly accessible but the diffusion coefficient measured for the *p*TsA tightly bound to the nanoparticles ($4.3 \times 10^{-10}\,m^2 s^{-1}$) represents a quite reasonable estimate because, even though their interaction is weaker, the hindered *p*TsA moves along with the nanoparticles when they are bound to them. $D_{f(X3)}$ is also not directly accessible but, as it corresponds to the free *p*TsA, the diffusion coefficient measured for the *p*TsA in the blank, corrected for the change of viscosity ($0.43 \times 36 \times 10^{-10}\,m^2 s^{-1}$), can be taken as a reasonable estimate. From these values $x_{f(X3)}$ and $x_{h(X3)}$ both turn out to be roughly 0.5. To summarize, the *p*TsA in X_3 can be split between three different types: the tightly bound ($\approx$50%), the weakly bound ($\approx$25%), and the free one ($\approx$25%), the latter two being in fast exchange on both the diffusion and chemical shift timescales.

A similar estimation can be performed for the ketonic acacH ligand, which does not display any tight bonding to the nanoparticles. The measured $< D >_{X3}$ equals $2.75 \times 10^{-9}\,m^2 s^{-1}$, and $D_{h(X3)}$ is approximated by the diffusion coefficient of the bound enolic acac ($3.4 \times 10^{-10}\,m^2 s^{-1}$) while $D_{f(X3)}$ is approximated by the diffusion coefficient of the free ketonic acacH in the blank, corrected from the viscosity change ($0.92 \times 3.60 \times 10^{-9}\,m^2 s^{-1}$). This estimation results in about 20% of the ketonic acacH interacting weakly with the nanoparticles and 80% as free as in the blank. For the enolic acac ligand, one obtains $x_{h(X3)} \approx 0.25$ which, together with the approximately 15% of tightly bound enolic acac ligand, represents more than a third of the enolic acac experiencing translational slowing down through strong, moderately strong, or weak interactions with the titanium oxide particles. In contrast, for *n*BuOH, on the basis of α-CH_2 and the CH_3 resonances, which are well isolated on the chemical shift scale, and therefore the most reliable resonances to be used, $x_{h(X3)} < 0.05$ confirms unambiguously that *n*BuOH plays a marginal role, if any, in the stabilization and tailoring of the nanoparticles.

For the sol S_3, only a limited number of data could be exploited from the spectra, because the large excess of *n*BuOH in this kind of sample causes dynamic range problems. The aromatic part of the 1D spectrum of the sol S_3 also exhibits resonances broader than those for the blank and X_3. The DOSY analysis of this system led to only one diffusion coefficient for every chemical species: $D_{TMS} = 25.4 \times 10^{-10}$, $D_{n\text{BuOH}} = 21.6 \times 10^{-10}$, $D_{\text{ketonic acacH}} = 22.3 \times 10^{-10}$, $D_{\text{enolic acacH}} = 25 \times 10^{-10}$, and $D_{p\text{TsA}} = 7.6 \times 10^{-10}\,m^2 s^{-1}$. For all species but the *p*TsA, the reduced diffusion coefficients ($\Delta_{n\text{BuOH}} = 0.88$, $\Delta_{\text{ketonic acacH}} = 0.91$, and $\Delta_{\text{enolic acacH}} = 1.02$) are remarkably similar to the ones in the blank (Table 1). Only the *p*TsA fraction, with a reduced diffusion coefficient of 0.31, is similar to the hindered/free *p*TsA fraction in X_3. It is thus the only ligand for which the interaction with the nanoparticles could be clearly revealed in S_3. The larger amount of acacH in S_3, as compared to X_3, does not allow the interaction with the nanoparticles to be visible any more.

DOSY NMR investigations in [D_4]methanol: With respect to [D_3]acetonitrile, changing the solvent to [D_4]methanol results in a significant loss of spectral resolution. *n*BuOH also exhibits a lower $\Delta_{(model)}$ than the other ligands, which can be logically ascribed to hydrogen bonding with the solvent molecules being stronger than for the other ligands (Table 2). Finally, the comparison of the reduced diffusion coefficients, between the blank and the models, indicates that mixing the ligands in [D_4]methanol slows down their diffusion with respect to the corresponding model solutions. In [D_3]acetonitrile, this effect was only observed for *p*TsA.

This result is quite normal, as the total concentration of solute molecules is higher in the blank than in each of the individual model solutions, and therefore all molecules are prone to more attractive intermolecular forces. This is also in line with *n*BuOH being a better hydrogen-bond donor than methanol.

For the xerosol X_3 in [D_4]methanol, several striking features can be outlined in the 1D ^{1}H NMR spectrum when compared to data in [D_3]acetonitrile. First, only relatively sharp doublets and a methyl singlet are observed for *p*TsA,

Table 2. Diffusion coefficients[a] [10^{-10} $m^2 s^{-1}$] and reduced diffusion coefficients, in [D_4]methanol, for the pure compounds (model solutions), blank sample, and redispersed xerosol X_3. The relative fractions are also given for species in different states (for example, free and bound).

Compounds		Model solutions		Blank		X_3		
		$D_{j(model)}$	$\Delta_{j(model)}$	$D_{j(blank)}$	$\Delta_{j(blank)}$	$D_{j(X3)}$	$\Delta_{j(X3)}$	%
*p*TsA	free	9.3	0.49	6.4	0.40			
	hindered/free					7.9	0.49	100
enolic 80 %	free acacH	22.1	1.06	14.6	0.92	15.7	0.97	85
	bound acac					2.4	0.15	15
ketonic 20 %	free acacH	20.8	1.00	13.2	0.83	15.8	0.98	100
*n*BuOH	free	14.6	0.75	10.4	0.65	14.7	0.91	100
TMS	free	20.3	1.00	15.9	1.00	16.2	1.00	100

[a] The relative accuracy of the diffusion coefficients is ±1 % for models, ±1 % for the blank, and ±10 % for X_3, and the relative accuracy of the fractions determined from DOSY NMR is ±10 % (see the Experimental Section).

without any additional broad resonances. The 2D DOSY spectrum confirms that no nanoparticle-bound *p*TsA is observed any more. No resonance related to the enolic form of acac is observed in the olefinic resonance range. This finding can readily be explained by the fact that the central vinylic proton of the enolic acac ligand can be substituted by the hydroxylic deuteron of [D_4]methanol. However, in the methyl range, the enolic form exhibits a single methyl resonance displaying two diffusion regimes, a fast and a slow one. According to the viscosity of the medium ($\eta = 0.75$ cP), the slower diffusion regime corresponds to a hydrodynamic radius of approximately 1.2 nm and is related to the enolic acac bound to the surface of the nanoparticles. As for [D_3]acetonitrile, the exchange between the bound and free enolic acac in [D_4]methanol is slow on the diffusion timescale. For [D_3]acetonitrile dispersions, only a single diffusion regime is observed for the ketonic tautomer of acacH and *n*BuOH (Table 2). All compounds show a faster diffusive behavior in the xerosol X_3 than in the blank, which is probably due to the smaller relative amount of *n*BuOH present in the former than in the latter. The main difference with respect to the xerosol X_3 in [D_3]acetonitrile is that, in [D_4]methanol, the bound *p*TsA ligands are now driven away from the nanoparticle surface. This feature is probably related to the esterification of the surface Ti–OH moieties by CD_3OD.

DOSY NMR investigations in [D_6]dimethyl sulfoxide: DOSY data on the blank and model solutions in [D_6]DMSO are gathered in Table 3. With respect to [D_3]acetonitrile (Table 1) and [D_4]methanol (Table 2), the mixing effect totally disappears upon changing the solvent to [D_6]DMSO, as all the reduced diffusion coefficients remain unchanged upon mixing.

Table 3. Diffusion coefficients[a] [10^{-10} $m^2 s^{-1}$] and reduced diffusion coefficients, in [D_6]DMSO, for the pure compounds (model solutions), blank sample, and redispersed xerosol X_3. The relative fractions are also given for species in different states (for example, free and bound).

Compounds		Model solutions		Blank		X_3		
		$D_{j(model)}$	$\Delta_{j(model)}$	$D_{j(blank)}$	$\Delta_{j(blank)}$	$D_{j(X3)}$	$\Delta_{j(X3)}$	%
*p*TsA	free	3.2	0.55	3.8	0.55			
	hindered/free					7.0	0.51	100
enolic 70 %	free acacH	9.4	1.08	7.9	1.14	7.0	1.00	85
	bound acac					2.4	0.35	15
ketonic 30 %	free acacH	8.5	0.98	6.9	1.00	7.0	0.99	100
*n*BuOH	free	7.0	0.88	6.2	0.88	6.3	0.89	100
TMS	free	7.0	1.00	7.0	1.00	7.0	1.00	100

[a] The relative accuracy of the diffusion coefficients is ±1 % for models, ±1 % for the blank, and ±10 % for X_3, and the relative accuracy of the fractions determined from DOSY NMR is ±10 % (see the Experimental Section).

amount than *p*TsA moieties, therefore overruling them in coordinating titanium at the nanoparticle surface, the strong complexing properties of DMSO towards metal atoms being well known. However, the two diffusion regimes of enolic acac(H) indicate that this strong coordination of DMSO does not drive the enolic acac ligand away from the nanoparticle surface. The diffusion behavior of *n*BuOH and ketonic acacH is not influenced by the presence of nanoparticles in [D_6]DMSO, which has nearly the same polarity as [D_3]acetonitrile.

DOSY NMR investigations in [D]chloroform: In $CDCl_3$, phase separation occurs in the *p*TsA model solution, blank and S_3 system. Accordingly, only the xerosol X_3 in $CDCl_3$ was investigated (Table 4).

The molecules in the X_3 xerosol in $CDCl_3$ have a nearly identical diffusive behavior to that in CD_3CN. Three different diffusion regimes are clearly distinguished: a free diffusion regime for both acacH tautomers and *n*BuOH, a bound diffusion regime for enolic acac and *p*TsA and a hindered/free diffusion regime for *p*TsA due to interactions, as already discussed for [D_3]acetonitrile. The similarity of these findings with those in the [D_3]acetonitrile dispersion is really striking, even for the thermodynamic fractions. Also, the hydrodynamic radius (≈2.5 nm) confirms the size of the nanoparticles already mentioned above for other solvents.

For the xerosol X_3 (Table 3), the enolic acac tautomer shows again two well-separated diffusion correlation peaks, indicating a free and a bound form. Differently from [D_3]acetonitrile, but similarly to [D_4]methanol, only a single diffusion regime is observed for *p*TsA in [D_6]DMSO, which is very similar to that of the blank. This is assigned to DMSO molecules which are present in a much larger

Table 4. Diffusion coefficients[a] [10^{-10} $m^2 s^{-1}$] and reduced diffusion coefficients, in $CDCl_3$, for the redispersed xerosol X_3. The relative fractions are also given for species in different states (for example, free and bound).

Compounds		X_3		
		$D_{j(X3)}$	$\Delta_{j(X3)}$	%
*p*TsA	hindered/free	7.2	0.32	50
	bound	2.2	0.10	50
enolic 60 %	free acacH	18.9	0.85	85
	bound acac	1.8	0.08	15
ketonic 40 %	free acacH	22.5	1.01	100
*n*BuOH	free	21.9	0.98	100
TMS	free	22.3	1.00	100

[a] The relative accuracy of the diffusion coefficients is ±10 % and of the fractions determined from DOSY NMR is ±10 % (see the Experimental Section).

This clearly illustrates that changing the polarity of the solvent, while keeping the viscosity almost constant, does not significantly alter either the global diffusive behavior of the organic compounds or the size characteristics of the nanoparticles in the system.

Conclusion

Diffusion-ordered NMR spectroscopy appears to be an elegant methodology to measure diffusion coefficients of organic structures interacting with nanoparticles. Coupling this technique to diffusion measurements on model solutions of these organic species provides valuable information on how their intrinsic translational mobility is altered in more complex nanoparticle dispersions. Thus, a systematic investigation going from model solutions to nanoparticle dispersions enables one to discriminate between solvation and interaction phenomena also present in model and blank solutions, and association/dissociation phenomena only present in the nanoparticle dispersion.

The analysis of 2D DOSY spectra, in both the chemical shift and diffusion dimensions, by using appropriate mathematical software tools for integration and deconvolution of the spectra or Gaussian decays, results in the quantification of thermodynamic fractions of the tautomeric equilibrium of acetylacetone and the dissociation/association equilibrium of the ligands at the surface of the nanoparticles. However, because of the ill-conditioned nature of inverse Laplace transformation (ILT), the fractions of the bound and free ligands should be considered with appropriate caution if the distinction of the species is only possible in the diffusion dimension of the 2D DOSY spectra as a consequence of identical chemical shifts.

Although a priori expected, the polarity does not influence significantly the behavior of the compounds in the nanoparticle dispersion, as clearly demonstrated by the very similar diffusion behaviors observed in [D]chloroform and [D_3]acetonitrile, which exhibit a dipolar moment/dielectric constant couple of 1.04 D/4.8, and 3.93 D/36.6, respectively.[20] The viscosity of the solvents determines the absolute values of the diffusion coefficients, but does not affect fundamentally the interaction behavior of the ligands at the nanoparticle surface. The only significantly different behavior is found for methanol, as a consequence of its specific hydrogen-bond donor capacities and ability to esterify the surface Ti–OH, with the result that the slow association/dissociation equilibrium of the *p*TsA ligand is speeded up.

Generally, all compounds show for all solvents, in model solutions as well as in the blank, diffusion characteristics which are similar to that of TMS; *p*TsA, the diffusion of which is hindered most likely by intermolecular interaction phenomena, constitutes a noticeable exception. In nanoparticle dispersions, the same free fractions and the hindered/free *p*TsA fraction are found, within experimental scatter. Furthermore, a nanoparticle-related diffusion regime is found for enolic acac and *p*TsA.

Every mixture component and diffusion regime was analyzed with different ^1H magnetic probes. In this way, all data are self-consistently cross-checked, thus confirming the reliability of the method, including data on the nanoparticle hydrodynamic radius of approximately 2 nm confirmed by DLS measurements. A global overview of the interaction and chemical-exchange model at the nanoparticle surface and in the bulk solution is given in Scheme 1.

It can be concluded that DOSY NMR is a powerful methodology enabling one to analyze qualitatively and semiquantitatively the thermodynamics and kinetics of interaction and exchange processes of organic ligands in all nanoparticle dispersions in different solvents. Undoubtedly, the methodology proposed goes far beyond the restricted frame of TiO_2 nanoparticles addressed here.

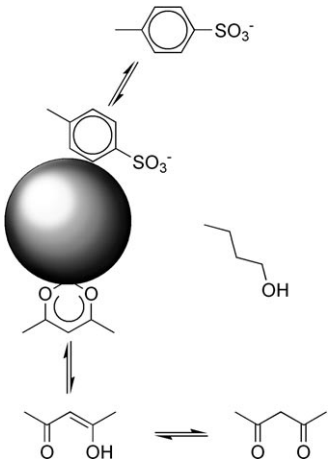

Scheme 1. Summarizing scheme of all possible equilibria and interactions between species in solution and nanoparticles in the dispersion mixture, as deduced from DOSY NMR spectroscopic data acquired from [D_3]acetonitrile dispersions.

Experimental Section

Synthesis: The sol S_3 and xerosol X_3 were prepared according to published procedures.[13a] For the sol S_3, Ti(O*n*Bu)$_4$ (1 equiv, 14.7 mmol) was added to a solution containing *n*BuOH (9 equiv, 132.3 mmol) and acacH

(3 equiv, 44.1 mmol). After stirring for 15 min, *p*TsA (0.2 equiv) in pure water (10 equiv) was added and the mixture was stirred for 2 h at room temperature, then heated at 65 °C for 24 h. For the corresponding xerosol X_3, the mixture was dried under vacuum for 4 h at approximately 0.01 mm Hg at room temperature, and subsequently overnight at 60 °C under atmospheric pressure, which provided a mass reduction of slightly above 90 %. For the blanks, a solution containing *n*BuOH (10 equiv, 147 mmol) and acacH (3 equiv, 44.1 mmol) was prepared. After stirring for 15 min, *p*TsA (0.2 equiv) in pure water (10 equiv) was added and the mixture was stirred for 2 h at room temperature, then heated at 65 °C for 24 h.

Instruments for NMR spectroscopy: Most ^{1}H NMR spectroscopic data were acquired on a Bruker Avance 250 spectrometer operating at 250.13 MHz. The spectral width was 3000 Hz, with an acquisition time of 1.36 s (digital resolution = 0.367 Hz per point), a recycling delay of 6.0 s and a 90° pulse width of 10.0 μs. The data were processed with an exponential broadening of 0.30 Hz. Some of the ^{1}H NMR spectroscopic data were acquired on a Bruker Avance II 700 spectrometer operating at 700.13 MHz. The spectral width was 9800 Hz, with an acquisition time of 3.34 s (digital resolution = 0.150 Hz per point), a recycling delay of 6.0 s, and a 90° pulse width of 7.0 μs. The data were processed with an exponential broadening of 0.60 Hz.

DOSY NMR measurements: Samples were prepared for NMR acquisitions by dissolving appropriate amounts in deuterated solvents (0.75 mL) containing TMS (3 μL) as a reference. The diffusion experiments were performed by pulsed field gradient (PFG) ^{1}H NMR spectroscopy by means of a BPP-LED pulse sequence,[21] with shaped gradient pulses of amplitude G and duration δ modulated as the $G[\sin(2\pi t/\delta)]$ function. Experiments were carried out at 300 K, without sample spinning, on a Bruker Avance 250 spectrometer equipped with a Bruker BGU z-gradient unit providing a maximum gradient of 51 G cm^{-1}. For each solution, the 1D spectra were acquired by using a BPP-LED pulse sequence to optimize the gradient pulse duration (δ) and the diffusion delay (Δ) in order to detect properly the full signal decay. The amplitude of the gradients was varied from 2 to 95 % of their maximum value, while the gradient recovery delay (τ) and the eddy current delay (t_e) were fixed at 1 and 5 ms, respectively. The diffusion delay (Δ) varied from 50 to 340 ms and the gradient pulse duration (δ) from 0.5 to 3.5 ms.

DOSY NMR data processing: The DOSY NMR data were processed by ILT,[22] by using a maximum entropy algorithm, MaxEnt,[23] as implemented in the Gifa Processing software interfaced with TOPSPIN software. The ILT–MaxEnt 2D DOSY spectra obtained in this way are represented on the vertical axis in f_1 as the negative logarithmic scale of the diffusion coefficient, and on the horizontal axis in f_2 as the chemical shift (in ppm), for each measurable moiety of the corresponding diffusing species. The resulting 3D spectrum was (numerically) integrated over a given resonance range along the chemical shift axis, which provides an intensity function depending only on the $-\log D$ variable. A sum of Gaussian functions was fitted to these data (see Figure 6) with different independent software packages (Excel, TableCurve, Perch), which increased the number of independent Gaussian distributions until (at least) two Gaussians equal within statistical error (clearly indicating that they represent the same diffusion regime) or the fraction of (at least) one Gaussian was reduced to zero (clearly indicating there are fewer diffusion regimes than represented by Gaussian distributions). The peak maxima thus obtained were used as the representative diffusion coefficients. The accuracy of the diffusion coefficients depends on the system. For spectra with no overlapping resonances, that is, models and blank, the ILT–MaxEnt 2D DOSY gave the same results as a simple monoexponential fitting, the accuracy of which is below 1 %.[24] For strongly overlapping systems, the accuracy of the diffusion coefficients determined by ILT–MaxEnt 2D DOSY can be estimated at ±10% by using a Monte Carlo approach.[25] However, the spread of the diffusion coefficients measured for the different resonances of a unique chemical species (for example, *p*TsA) was always narrower. With the same Monte Carlo approach, the accuracy of the fractions of the different components is also estimated as ±10 %.[25]

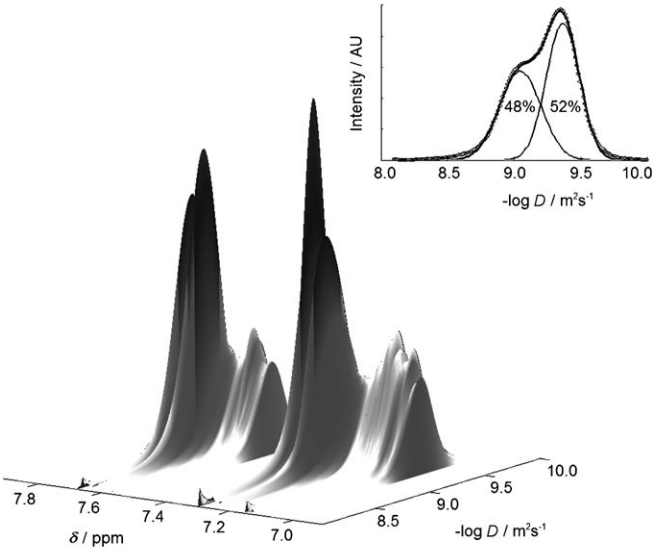

Figure 6. Stacked plot of the aromatic spectral range of the 2D DOSY spectrum of the xerosol X_3 redispersed in [D_3]acetonitrile. The plot clearly shows the less intense, broader (along the chemical shift scale) peaks of *p*TsA ligands bound to nanoparticles. The deconvolution shown in the inset was performed on the projection resulting from summing up all cross sections parallel to the diffusion axis of the 2D DOSY spectrum within the chemical shift range $\delta = 7.0$–7.8 ppm.

Viscosity measurements: For the three types of samples analysed in each solvent, the blank, the sol (S_3), and the re-dispersed xerosol (X_3), the actual dynamic viscosity of the medium was determined by using TMS as an internal reference.[26] TMS appeared particularly appropriate for this purpose, as it is inert, nonpolar, and nonpolarizable, and therefore hardly interacts with any of the substrates of interest, including the solvent. This leads to the reasonable assumption that the product of its hydrodynamic radius (r_H) and the parameter c of the Stokes–Einstein relation is constant in a given solvent. The viscosities of the pure deuterated solvents were taken from Holz et al.[27] A complete list of viscosities is given in the Supporting Information.

^{1}H NMR spectroscopic data (250 MHz): For all the studied samples, chemical shifts, integrals, homonuclear proton scalar coupling constants, and assignments are given in the Supporting Information.

Acknowledgements

The authors wish to thank Professor M. A. Delsuc (Université de Montpellier I) for helpful discussions concerning the MaxEnt implementation of the ILT. Financial support by the fund of Scientific Research Flanders (Belgium) (FWO; Grants G.0016.02 and G.0469.06) and the Research Council (Onderzoeksraad) of the Vrije Universiteit Brussel (Concerted Research Action, Grant GOA31) to R.W., L.V.L., G.M., and M.B. is gratefully acknowledged. V.E. is indebted to the fund of Scientific Research Flanders (Belgium) (FWO) for a postdoctoral foreign fellowship. R.W. and J.C.M. acknowledge the financial support by the fund of Scientific Research Flanders (Belgium) (FWO; Grant G.0064.07). The FWO Scientific Research Network on Magnetic Resonance is gratefully acknowledged for financially facilitating exchange of researchers between the different labs involved in this work (Grant WO.01407). The "Ministère des affaires Etrangères" is acknowledged for its support through the PHC-Tournesol No. 11537UF.

[1] a) B. Antalek, *Concepts Magn. Reson.* **2002**, *14*, 225–258; b) S. Abrahmsen-Alami, P. Stilbs, *J. Colloid Interface Sci.* **1997**, *189*, 137–143; c) C. S. Johnson Jr, *Prog. Nucl. Magn. Reson. Spectrosc.* **1999**, *34*, 203–256.
[2] a) L. H. Lucas, W. H. Otto, C. K. Larive, *J. Magn. Reson.* **2002**, *156*, 138–145; b) W. S. Price, H. Ide, Y. Arata, *J. Phys. Chem. A* **2003**, *107*, 4784–4789.
[3] P. Groves, M. O. Rasmussen, M. D. Molero, E. Samain, F. J. Canada, H. Driguez, J. Jimenez-Barbero, *Glycobiology* **2004**, *14*, 451–456.
[4] O. Söderman, P. Stilbes, *Prog. Nucl. Magn. Reson. Spectrosc.* **1994**, *26*, 445–482.
[5] M. Valentini, P. S. Pregosin, H. Ruegger, *Organometallics* **2000**, *19*, 2551–2555.
[6] C. Roberts, T. Cosgrove, R. G. Schmidt, G. V. Gordon, *Macromolecules* **2001**, *34*, 538–543.
[7] P. Bernado, J. Garcia de la Torre, M. Pons, *J. Mol. Recognit.* **2004**, *17*, 397–407.
[8] a) M. J. Stchedroff, A. M. Kenwright, G. A. Morris, M. Nilsson, R. K. Harris, *Phys. Chem. Chem. Phys.* **2004**, *6*, 3221–3227; b) M. Nilsson, I. F. Duarte, C. Almeida, I. Delgadillo, B. J. Goodfellow, A. M. Gil, G. A. Morris, *J. Agric. Food Chem.* **2004**, *52*, 3736–3743; c) A. R. Bilia, M. C. Bergonzi, F. F. Vincieri, P. Lo Nostro, G. A. Morris, *J. Pharm. Sci.* **2002**, *91*, 2265–2270; d) R. K. Harris, K. A. Kinnear, G. A. Morris, M. J. Stchedroff, A. Samadi-Maybodi, N. Azizi, *Chem. Commun.* **2001**, *23*, 2422–2423; e) P. Hodge, P. Monvisade, G. A. Morris, I. Preece, *Chem. Commun.* **2001**, *3*, 239–240.
[9] F. Ribot, V. Escax, J. C. Martins, M. Biesemans, L. Ghys, I. Verbruggen, R. Willem, *Chem. Eur. J.* **2004**, *10*, 1747–1751.
[10] J. M. Santos, R. Ribeiro da Silva, A. L. Formiga, L. W. Tinoco, J. D. Figueroa-Villar, *Chem. Phys.* **2004**, *306*, 143–151.
[11] F. Ribot, V. Escax, C. Roiland, C. Sanchez, J. C. Martins, M. Biesemans, I. Verbruggen, R. Willem, *Chem. Commun.* **2005**, 1019–1021.
[12] a) Z. Hens, I. Moreels, J. C. Martins, *ChemPhysChem* **2005**, *6*, 2578–2584; b) I. Moreels, J. C. Martins, Z. Hens, *ChemPhysChem* **2006**, *7*, 1028–1031.
[13] a) E. Scolan, C. Sanchez, *Chem. Mater.* **1998**, *10*, 3217–3223; b) E. Scolan, C. Magenet, D. Massiot, C. Sanchez, *J. Mater. Chem.* **1999**, *9*, 2467–2474.
[14] D. T. Cromer, K. Herrington, *J. Am. Chem. Soc.* **1955**, *77*, 4708–4709.
[15] a) E. J. Cabrita, S. Berger, P. Bräuer, J. Kärger, *J. Magn. Reson.* **2002**, *157*, 124–131; b) E. J. Cabrita, S. Berger, *Magn. Reson. Chem.* **2002**, *40*, S122–S127.
[16] D. Canet, M. Decorps in *Dynamics of Solutions and Fluid Mixtures by NMR* (Ed.: J. J. Delpuech), Wiley, Chichester, **1995**, pp. 336–340.
[17] D. Zuccaccia, A. Macchioni, *Organometallics* **2005**, *24*, 3476–3486.
[18] E. J. Cabrita, S. Berger, *Magn. Reson. Chem.* **2001**, *39*, S142–S148.
[19] From the molecular structure of acacH and *p*TsA, the average atomic distance to their geometric centre can be calculated at 2.5 and 2.2 Å for *p*TsA and acacH, respectively. The maximum distance to their geometric centre can be similarly calculated at 3.8 and 3.2 Å for *p*TsA and acacH, respectively. In conclusion, both molecules exhibit a similar size.
[20] *CRC Handbook of Chemistry and Physics*, 82nd ed., CRC Press, Boca Raton, **2001**.
[21] D. Wu, A. Chen, C. S. Johnson Jr. , *J. Magn. Reson. A* **1995**, *115*, 260–264.
[22] a) R. Huo, R. Wehrens, J. van Duynhoven, L. M. C. Buydens, *Anal. Chim. Acta* **2003**, *490*, 231–251; b) B. Antalek, J. M. Hewitt, W. Winding, P. D. Yacobucci, T. Mourey, K. Le, *Magn. Reson. Chem.* **2002**, *40*, S60–S71.
[23] F. Mariette, J. P. Guillement, C. Tellier, P. Marchal in *Signal Treatment and Signal Analyses in NMR* (Ed.: D. N. Rutledge), Elsevier, Amsterdam, **1996**, pp. 218–234.
[24] M. Nilsson, M. A. Connell, A. L. Davis, G. A. Morris, *Anal. Chem.* **2006**, *78*, 3040–3045.
[25] M. A. Delsuc, T. E. Malliavin, *Anal. Chem.* **1998**, *70*, 2146–2148.
[26] E. J. Cabrita, S. Berger, *Magn. Reson. Chem.* **2001**, *39*, S142–S148.
[27] M. Holz, X. Mao, D. Seiferling, A. Sacco, *J. Chem. Phys.* **1996**, *104*, 669–679.

Received: December 1, 2006
Published online: June 12, 2007

